COLD SEA SURFACE TEMPERATURE NEAR CHEJU ISLAND RESPONDING TO STRONG CYCLONIC WIND AND POSITIVE GEOPOTENTIAL TENDENCY BEHIND A TYPHOON CENTER ALONG ITS TRACK

Hyo Choi[1], Mi-Sook Lee[2], and Soo Min Choi[3]

ABSTRACT

The response of sea surface temperature (SST) before and after the passage of Typhoon-18 Songda in the vicinity of Chjeu Island in the southern sea of Korea was investigated using satellite-derived GOES-MCSST (SST), GOES infrared cloud image and a three dimensional WRF-3.0 model with FNL initial meteorological data on September 5 to 8, 2004. On September 4, before the typhoon passed by Cheju Island, the SST extending southwards and eastwards of the island was 27°C. However, after the typhoon passed by the island at 2100 LST, September 7, the SST decreased by 2°C to 25°C. Asymmetrical-cyclonic surface wind generated by the combination of the movement of the typhoon and the cyclonic winds of the typhoon itself, caused divergence of wind driven currents, which induced upwelling of deep sea colder water to the sea surface and outward spreading of cold waters near the island. This resulted in the decrease of SST and a negative maximum geopotential tendency of 500 hPa for 24 hours ($\partial\Phi/\partial t$; m/day) was detected in the center of the typhoon eye, where the thinner atmospheric layer existed. This induced a decrease in the sea surface height and in the downwelling of surface waters. A positive maximum geopotential tendency was detected behind the typhoon center along its track, where maximum expansion of the atmospheric depth caused the level of the sea surface to rise and upwelling of deep sea cold waters to the surface. Thus, the slope height ranging from 422 to 639 m/day between two maxima of geopotential tendencies could strongly influence the sea surface elevation, thereby inducing a very strong upwelling and outward spreading of deep sea colder waters toward the inclined sea surface, resulting in a decrease of SST in the wake of the typhoon track.

I. INTRODUCTION

Tropical cyclones (also called typhoons in the northeast Asia and hurricanes in the North Atlantic and North Pacific) occur frequently in summer and cause disasters relating to strong winds and severe flooding due to heavy precipitation and storm surges [1, 3]. Gill [9], Kantha and Clayson [12] and Sheng *et al.* [22] showed that hurricane-induced upwelling is observed a few days after the passage of a hurricane accross the Gulf of Mexico and Ekman trasport occurs from the path of the storm center on the storm track, resulting in horizontal displacements of particles in the surface layer of some tens of kilometers and upwelling of waters along the storm axis by some tens of meters vertically.

Price [16], Monaldo *et al.* [15], Cione and Uhlhorn [6], Elsner [7] and Knauss [13] concluded that cyclonic surface winds in a hurricane result in upwelling of bottom colder waters to the sea surface, because the surface wind stress can cause surface divergence of sea surface water and upwelling of bottom colder water toward the sea surface in the open ocean by the changes in wind speed or direction in the wake of a hurricane. By upwelling process, nutrient-laden waters can greatly affect coastal fisheries with aquaculture and environmental stressors in marine ecosystems [2, 8].

Using Weather Research and Forecasting Model (WRF)-version 3.0, the atmospheric pressure change of a Typhoon-Songda and strong cyclonic surface wind were investigated
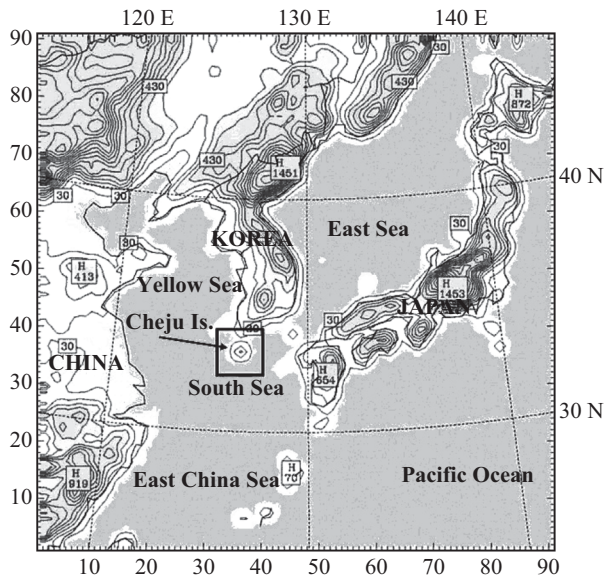
Fig. 1. Topographical features adjacent to Korean peninsula (large box) and Cheju Island (small box) for WRF model simulation.

Fig. 2. Track of Typhoon-18, Songda on August 27~September 8, 2004.

before and after the typhoon passage near Cheju Island in Korea over the period of September 6 to 8, 2004. Geostationary Operational Environmental Satellite (GOES)-Infrared image of cloud and surface weather maps were used for tracking of typhoon passage, and daily mean sea surface temperature (SST) data of GOES-Multi-Channel Sea Surface Temperature (MCSST) were also used to assess the variation of SST responding to both atmospheric pressure change of the typhoon and the strong cyclonic surface winds.

II. STUDY AREA

The study area is near Cheju Island (W-E: 73 km; S-N: 41 km) which is the largest island in Korea and has a bell type topography covering an oval shaped area in the south of Korean peninsula. Its climate is greatly affected by the Yellow Sea Warm Current passing by Cheju Island and along the Korean west coastal sea and the East Korea Warm Current between the Korean peninsula and Japan Island in the east (Fig. 1).

The sea adjacent to Cheju Island is sallower at less than 100 m in the west, north and east of the smaller square domain in Fig. 1 and relatively deeper at greater than 100 m to 300 m in the south, close to the East China Sea. In summer, most of typhoons pass near this island reaching the Korean peninsula or Japan islands.

III. NUMERICAL METHOD AND INPUT DATA

A three dimensional WRF-3.0 model with a terrain following coordinate system was adopted for the generation of wind, precipitation, cloud and 500 hPa height change for 24 hours (i.e., geopotential tendency ($\partial\Phi/\partial t$; m/day) near Cheju
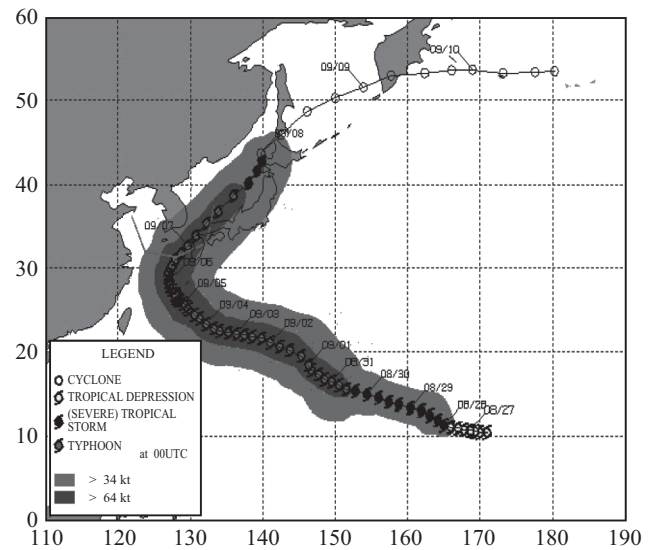
Island [11]. Numerical simulation by the model was carried out from 0000 UTC (Local Stand Time (LST) = 9h + UTC), September 5 through 2100 UTC, September 7, 2004. In the numerical simulation, one way, triple nesting process from a coarse-mesh domain to a fine-mesh domain was performed using a horizontal grid spacing of 27 km covering a 91×91 grid square in the coarse mesh domain.

The second and third domains also consist of the same grid square of 91×91 with 9 km and 3 km horizontal grid intervals. National Centers for Environmental Prediction/National Center for Atmospheric Research (NCEP/NCAR) reanalysis-Final Analyses (FNL) $1.0° \times 1.0°$ resolution data were used as meteorological input data to the model and were vertically interpolated onto 36 levels with sequentially larger intervals increasing with height from the surface to the upper boundary level of 100 hPa [4, 5]. Hourly archived data set of wind, air temperature, relative humidity, cloud and geopotential tendency by Cheju Meteorological Office were used for the verification of numerical results of meteorological elements.

IV. RESULTS AND DISCUSSION

1. Typhoon Track and Synoptic Situation

At 1100 UTC, August 26, 2004, Joint Typhoon Warning Centre, USA (JTWC) reported a new area of convection which had developed and persisted approximately 210 nautical miles northeast of Kwajalein (Fig. 2). JTWC at 1200 UTC, August 27 gave the first warning on Tropical Depression-22W with its center at 270 nautical miles east of Eniwetak atoll in the Pacific Ocean and at 0000 UTC, August 28, the tropical depression with its surface wind speed of 35 kts was assigned the name as Songda as a tropical storm. At 1800 UTC, August 30, it became a typhoon with maximum surface wind speed of 95 kts and it situated about 17 nautical miles
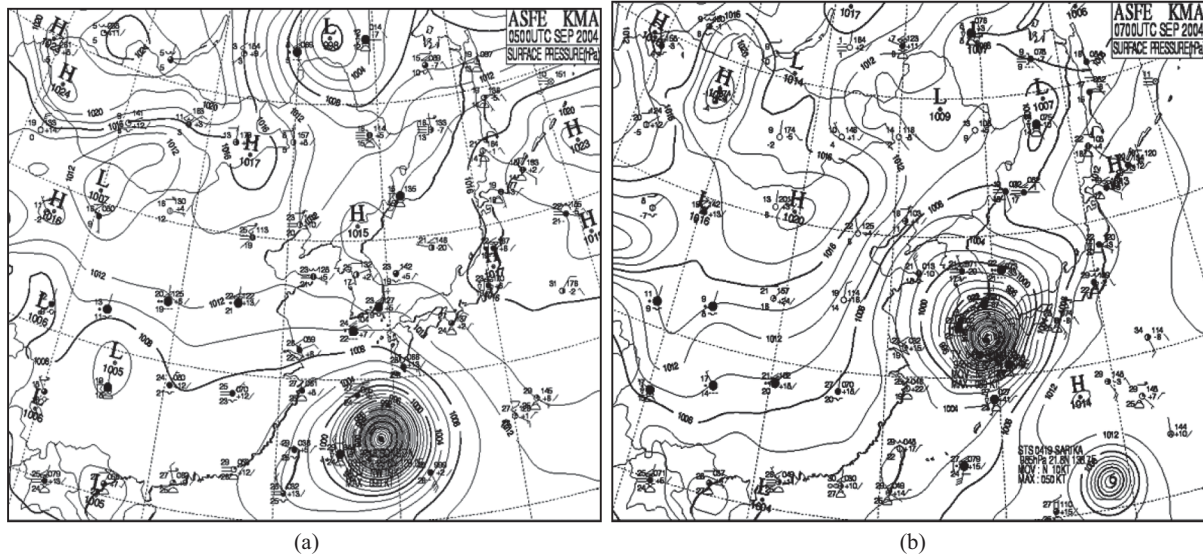
Fig. 3. (a) Surface weather map at 0900 LST (0000 UTC), September 5, 2004 before Typhoon Songda passed by Cheju Island, in the south of Korea and (b) 0900 LST (0000 UTC), September 7, after it passed by the right hand side of the island.
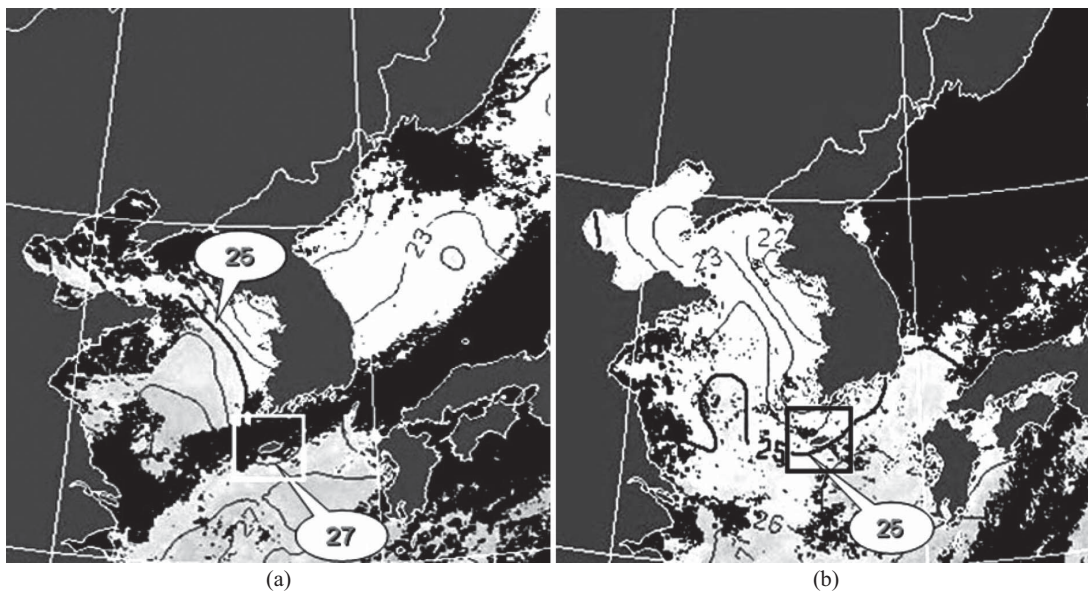

Fig. 4. (a) Daily mean of sea surface temperature (SST; 27°C near Cheju Island-small white box) by GOES-9 MCSST satellite images of Japan Meteorological Agency, September 4, 2004, before the typhoon passage and (b) September 7 (25°C) after its passage, respectively. The SST image on September 5 was not detected due to clouds, but one on September 4 was used. Wide black area in the sea denotes cloud covered area.

north-northeast of Agrigan Island in the Northern Mariana Islands at 0300 UTC, September 1. The typhoon moved north-westward continuously until September 4.

At 0000 UTC (0900LST), September 5, its strength began to weak and at 0000 UTC, September 7, as Typhoon Songda, it changed its direction to northeastward across the East China Sea and made landfall on the northwestern coast of Kyushu Island, Japan. Cheju Island, Korea to the left of Kyushu Island was in the strong impacted by the typhoon (Figs. 3(a) and (b)). At 1800 UTC, September 7, its strength began to

slowly decrease and was downgraded to a tropical storm and at 0600 UTC, September 8, when it became an extra-tropical cyclone (i.e., a low pressure).

2. Cold Water Outbreak Under Changes of Surface Wind Fields

On September 4, before the typhoon passed by Cheju Island, satellite-derived SST near the island was 27°C (Fig. 4(a)). However, at 2100 LST, September 7, after the island including Korean peninsula was entirely out of the influence
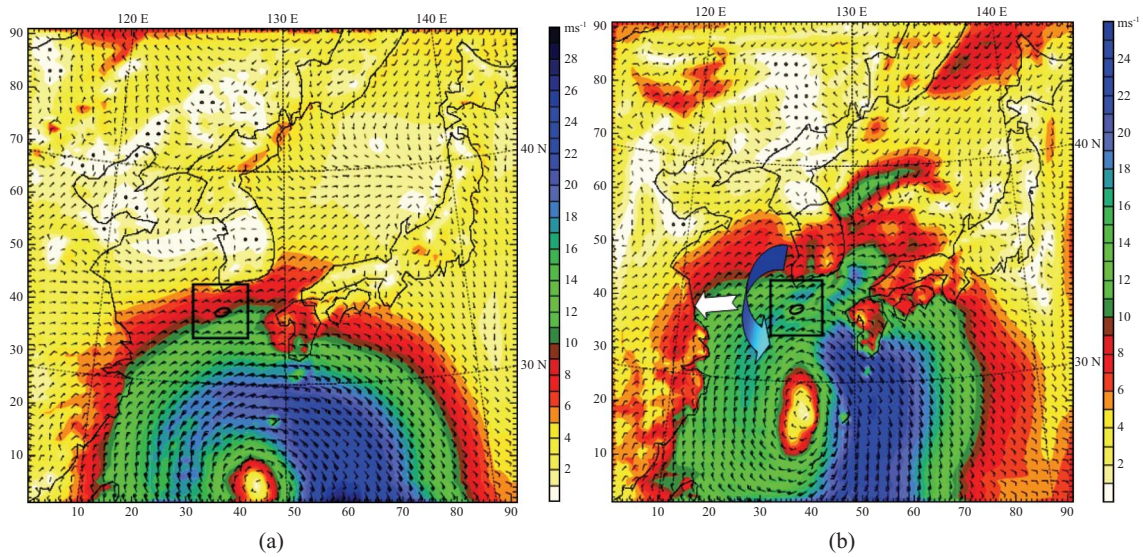
Fig. 5. Surface winds (m/s) in (a) a coarse-mesh domain with a 27 km horizontal grid interval at 0900 LST, September 5, 2004, before a typhoon-Songda passed by Cheju Island, where a box denotes the vicinity of Cheju Island, and (b) at 0900 LST, September 6. A small circle in the typhoon boundary in the south of Cheju Island in (a) denotes typhoon eye with calm or very weak wind. Large white and curved arrows denote wind driven current and cyclonic winds, respectively.
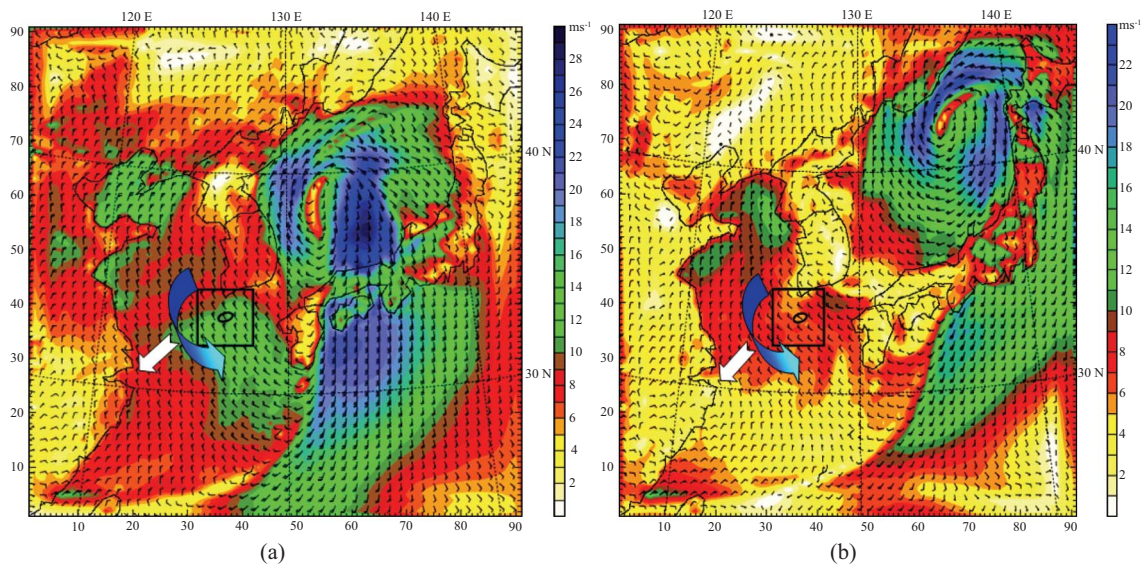

Fig. 6. As shown in Fig. 5, except for (a) at 0900 LST, September 7, 2004, when the typhoon just passed by the right hand side of Cheju Island (small box) and (b) at 2100 LST, September 7, after the weakening and splitting of the typhoon due to land and shallower sea depth and becoming an extra-tropical cyclone (i.e., a low pressure) in the East Sea of Korea. Large white and curved arrows denote wind driven current and cyclonic winds, respectively.

of the typhoon, the SST was then 25°C in the coastal sea on the southern side of the island, indicating a 2°C decrease (Fig. 4(b)). It is known that upwelling or downwelling occurs in the open ocean where winds cause surface waters to diverse or move away from a region, and hence upwelling, where convergence occurs toward a region and thus downwelling.

At 0900 LST, September 5, Cheju Island was just starting to be influenced by Typhoon Songa (Fig. 5(a)). At 0900 LST, September 6, the following day before the typhoon made

landfall on the northwestern coast of Kyushu Island, Japan, marine surface wind by cyclonic circulation of the typhoon near Cheju Island was greater than 20 m/s (Fig. 5(b)). In Fig. 6(a) at 0900 LST, September 7, Cheju Island was under the strong influence of the typhoon, which was weakened and divided into two regimes due to land and shallower sea depth, close to Korean peninsula and Kyusu Island, Japan.

Figs. 5(a) and (b) show that cyclonic surface winds were the strongest in the east and south of Cheju Island, with an

asymmetrical distribution due to the combination of the typhoon movement and cyclonic wind generated by the typhoon itself. The asymmetrical-cyclonic maximum wind can maximize surface divergence of wind driven current normal to the wind and result in upwelling of deep colder sea waters up to the sea surface. Thus, in Fig. 4(a), relatively cold sea waters of daily mean SST of 22°C near Inchon coastal sea of Korea and 25°C in the central part of the Yellow Sea, were transported southward by strong wind driven currents and further south of Cheju Island as shown in Fig. 4(b) at 0900 LST, September 7, one day after the typhoon's passage. The resulting SST distribution is attributed to the response to upwelling by the tropical cyclonic wind forcing and the wind driven current.

The cyclonic marine surface winds in our numerical simulation result using WRF model were able to generate divergence of ocean surface currents outward from the typhoon eye in relatively weak or calm wind field. Then, resulting outward divergent current could induce upwelling of deep colder water to the sea surface. The upwelling colder waters could spread outward around Cheju Island, resulting in the SST decrease of 2°C. This trend continued until the island was entirely out of the typhoon influence at 2100 LST, September 7 (Figs. 6(a) and (b)).

However, in contrast to an extra-tropical cyclone (weaker), the speed of movement of Typhoon Songda passing by Cheju Island was 6 to 7 m/s and cyclonic surface wind speeds generated by the typhoon itself were 5 to 22 m/s, resulting in surface winds to be 10 to 30 m/s. Using Ekman vertical displacement formula by Gill [9] and Leipper [14] on the hurricane-induced upwelling normal to the storm track, corresponding ocean current speeds were in the range of 0.15 to 0.66 m/s. Thus, the rising sea surface could reach more than 40m, and colder sea waters below 40 m depth could ascend to the sea surface and spread outward, as shown by the cold water outbreak around Cheju Island (Fig. 4(b)).

3. Upper Ocean Response to Temporal Variation of Geopotential Height in the Atmosphere

Another significant thing is that temporal variation of 500 hPa height (approximately atmospheric depth of 5 km) for 24 hours called geopotential tendency ($\partial \Phi/\partial t$; m/day) indicates the atmospheric depth at the 500 hPa level to the ground surface to be vertically shrunken or expanded [17]. Reed and Albright [18], Reed and Sanders [19], Sanders and Gyakum [21] and Holton [10] insisted that at the 500 hPa level, the area of the maximum positive geopotential tendency (+ $\partial \Phi/\partial t$) coincides with the area of maximum negative vorticity which induces the strong upward motion of air and vice versa. Divergence of surface winds associated with the subsidence of vertical circulation of air contributes a positive vorticity tendency at the 500 hPa trough and a negative vorticity tendency at the 1000 hPa (around the ground surface). That is, in the region of negative vorticity advection in the left hand side of trough of upper cold low, a positive vorticity tendency with
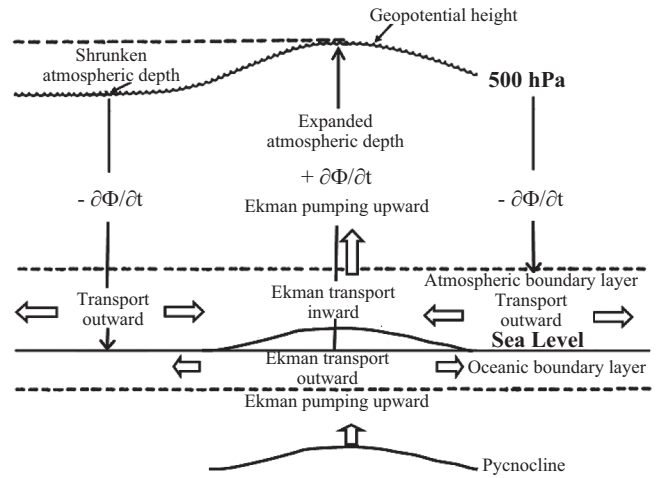

Fig. 7. Schematic profile of geopotential tendency ($\partial \Phi/\partial t$; m/day). Expansion of atmospheric depth by positive geopotential tendency over the sea surface induces the elevation of sea surface, which causes upwelling of deep cold sea waters toward the sea surface and outward spreading along the inclined sea surface (modified after Choi [4] and Gill [9]).

convergence of air in the upper level induces the downward motion of air toward the ground surface, also causing strong surface wind with diverging winds near the ground surface. According to Bernoulli theory, the fluid velocity in a channel is inversely proportional to vertical cross sectional area [20], and a much shrunken atmospheric depth produces a strong channel flow or wind.

From vorticity theory, a positive vorticity at 500hPa causes convergence of air in the upper level and results in low values of geopotential height (Φ) and vice versa. Thus, the region of positive vorticity at 500 hPa inducing downward motion of air toward the ground surface matches the region of negative geopotential tendency (- $\partial \Phi/\partial t$). Hence, the region of negative geopotential tendency implies the region of vertically shrunken atmospheric depth between the 500 hPa and ground surface levels for 24 hours, while the region of positive one matches the region of expanded atmospheric depth (Fig. 7).

Gill [9] explained that convergence of mass in some places leads fluid to be sucked vertically into the boundary layer of the earth's surface to replace that which is lost across the sides and this effect is called Ekman transport. Thus, the Ekman transport of air in the atmospheric boundary layer is toward the convergence of air masses (Ekman transport inward) and the Ekman pumping velocity outside the atmospheric boundary layer gives ascending motion of air (convection). Thus, the ascending motion of air causes the increase of atmospheric depth with time (i.e., positive geopotential tendency at 500 hPa level) to replace the converging air in the atmospheric boundary layer.

In the ocean underneath, that is, in the oceanic boundary layer, the Ekman transport of water is outward (divergence) along the inclined sea surface, away from the center of convergence of air and the ascending motion of air on the sea
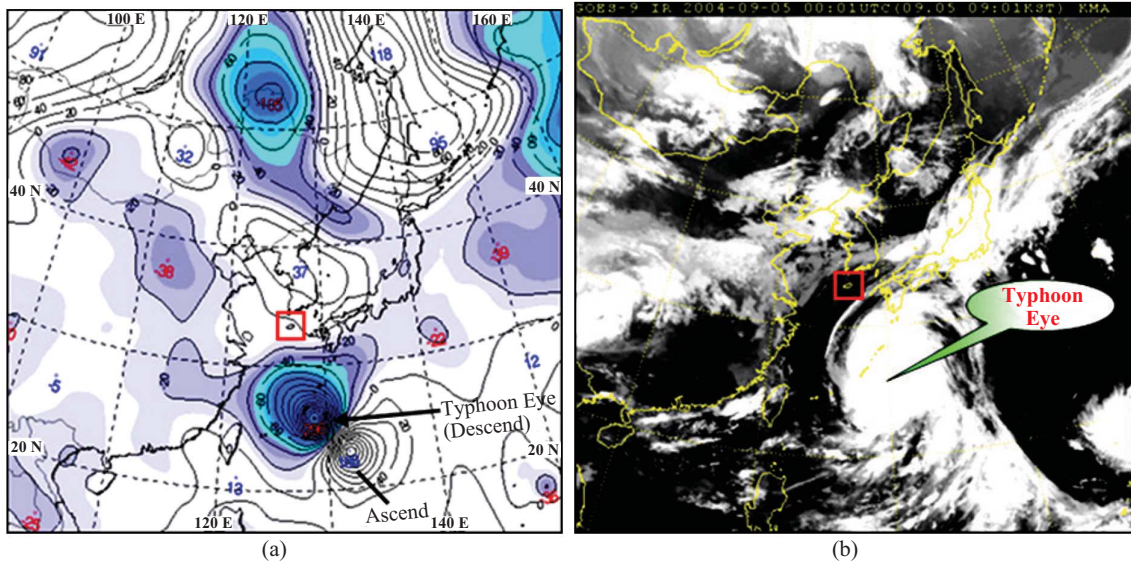
Fig. 8. **(a) Geopotential tendency (∂Φ/∂t; m/day) over the sea and land surfaces, before the passage of Typhoon Songda near Cheju Island (a small square) at 0900 LST, September 5, 2004 and (b) GOES-9 satellite infrared cloud image. White (blue) color area near Cheju Island denotes the increase (decrease) of geopotential tendency with a maximum of +188 m/day (-296 m/day) and a slope height of 483 m/day between two maxima induces ascent of sea surface, resulting in upwelling of deep colder waters upward and vise versa. A negative maximum geopotential tendency area was found in typhoon eye, but a positive one behind the typhoon along its track, respectively.**
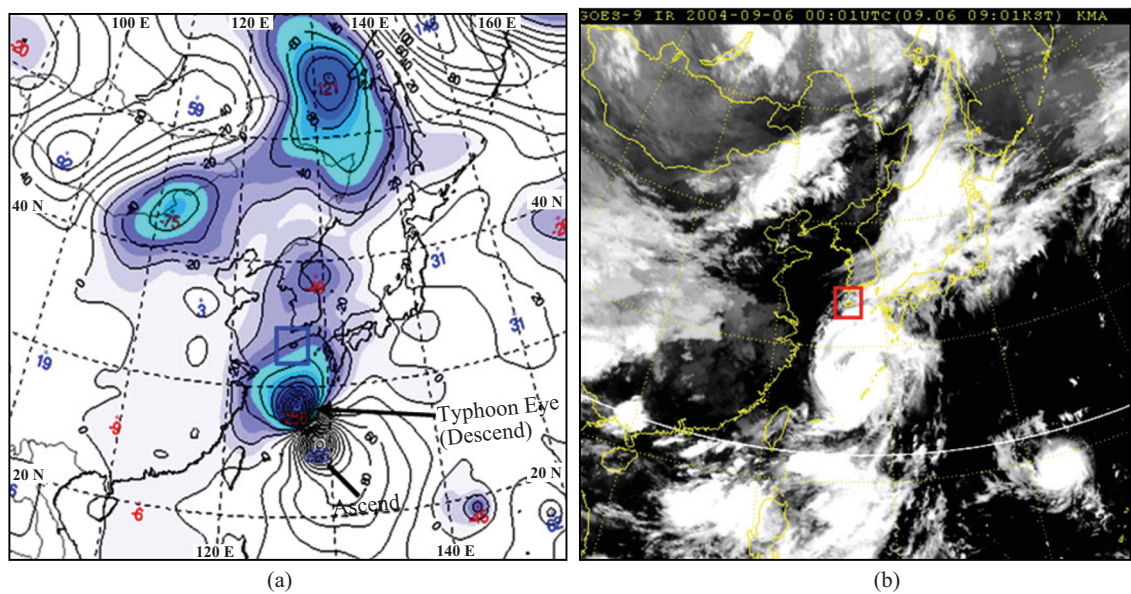

Fig. 9. **As shown in Fig. 8, except for (a) 500 hPa height change for 24 hours at 0900 LST, September 6, 2004 and (b) GOES-9 satellite infrared cloud image. White (blue) color area near Cheju Island denotes the increase (decrease) of geopotential tendency with a maximum of +166 m/day (-256 m/day) and a slope height of 422 m/day between two maxima.**

surface. Thus, the Ekman transport outward in the oceanic boundary layer induces upwelling of deep cold sea waters generated by an upward Ekman pumping velocity from the lower level toward the sea surface and outward spreading cold sea waters toward the vicinity, resulting in the decrease of sea water temperature (Fig. 7).

Oppositely, there must be the downward motion of air in the region of decreasing atmospheric depth with time at the 500 hPa level (i.e., negative geopotential tendency) to replace the diverging air in the atmospheric boundary layer near the sea surface. This divergence of air induces convergence of sea waters in the oceanic boundary layer downward and the decrease of the sea surface elevation, which causes downwelling of surface waters. Thus, most significantly, the increase (decrease) in temporal variation of the 500 hPa height (approximate 5,000 m atmospheric depth) for 24 hours over the

sea surface can induce ascent (decent) of the sea surface, resulting in upwelling (downwelling) of colder deep waters upward (relatively warmer surface waters downward).

On September 5, the area of a negative maximum geopotential tendency of – 296 m/day (blue area) in Fig. 8(a) corresponded to the typhoon eye, which was also seen in the center of the typhoon on GOES-9 satellite infrared cloud image in Fig. 8(b). A negative maximum geopotential tendency of – 296 m/day (blue color area) in typhoon eye (Fig. 8(a)), which is more deepened than 12 hours before, causes more strong positive vorticity at 500 hPa level and can induce the atmospheric layer to decrease, resulting in descent of the sea surface and downwelling of surface waters.

Otherwise, a positive geopotential tendency of +5 m/day (white area) was detected near Cheju Island, in the southern sea of Korea (a small square) with its maximum of +188 m/day behind the typhoon center along its track, and where a maximum expansion of atmospheric depth existed. Thus, the slope height of 483 m/day between two maxima could strongly drive the sea surface elevation, which might induce upwelling and outward spreading of deep sea colder waters along the inclined sea surface and result in cooling of sea surface waters such as decreasing of sea surface temperature in the wake of the typhoon track.

Similarly, at 0900 LST, September 6, a negative maximum geopotential tendency of – 256 m/day (blue area) in Fig. 9(a) was still detected in typhoon eye on GOES infrared cloud image (Fig. 9(b)). The area of negative maximum geopotential tendency corresponded to the existence of the thinner atmospheric layer, resulting in descent of the sea surface and downwelling of surface waters. On the other hand, a positive maximum geopotential tendency of +166 m/day was detected behind the typhoon center along its track, where a maximum expansion of atmospheric depth existed, resulted in upwelling of deep colder waters up to the sea surface. Thus, the slope height of 422 m/day between two maxima could strongly affect the sea surface elevation, and induced upwelling of deep sea colder water into the sea surface. As a result, cooling of the sea surface temperature in the wake of the typhoon track occurred as shown in Fig. 4(b).

At 0900 LST, September 7 in Figs. 10(a) and (b), the typhoon turned toward northeast and passed by Korea Strait. The northwestward track of the typhoon also changed a northeastward track. A negative maximum geopoential tendency of -316 m/day (blue color area), which could potentially decrease the atmospheric depth, was still detected near the typhoon center, thereby causing the drop in sea surface level and downwelling of surface waters. Consequently, behind the typhoon center on its track, a positive maximum geopotential tendency of +317 m/day (white color area) occurred, inducing expansion of the atmospheric depth. That drove a rise in the sea surface level, thereby inducing upwelling and outward spreading deep sea colder water along the inclined sea surface. The slope height between two maxima of negative and positive tendencies reached 633 m/day and this intense slope

forced more deep sea cold water toward the sea surface, resulting in continuous cooling of the sea surface temperature in the wake of the typhoon.

As shown in Fig. 6(a), around 0900 LST, September 7, with Typhoon-Songda passing by the right hand side of Cheju Island (small square), the typhoon lost its structure owing to a shallower sea depth close to the Korean peninsula and Kyusu Island, Japan by dividing into two air masses, and then becoming a tropical depression. As it further passed trough the Korean Strait between Busan city in the southeastern edge of the Korean peninsula and Kyusu Island, Japan, it further split into three air masses at 2100 LST September 7, as shown in Fig. 6(b). Finally, the tropical depression became an extra-tropical cyclone (i.e., a low pressure system) over the East Sea of Korea.

At 2100 LST, September 7, it can be seen that the tropical depression became an extra-tropical cyclone (a low pressure system) over the East Sea of Korea (The Sea of Japan) as shown in the GOES-9 satellite infrared cloud image (Fig. 11(b)). In Fig. 11(a), a negative maximum geopoential tendency of -276 m/day meant that a decreased atmospheric depth could still be detected near the center of the low pressure system which caused the drop in the sea surface level and downwelling of surface waters.

On the other hand, a positive maximum geopotential tendency of +363 m/day to the south of Cheju Island meant that upwelling of deep cold sea waters could be produced by the expansion of the atmospheric layer. The slope height of 639 m/day between two maxima of negative and positive tendencies produced a rise in the level of the sea surface, resulting in upwelling and outward spreading of deep colder waters upward from the maximum ascent of sea surface along the inclined sea surface. Thus, as the colder sea waters spread out to the southeast of Cheju Island near the maximum rise in the level of the sea surface, the SST of 27°C just near the island cooled by 2°C to 25°C (Fig. 4(b)).

V. CONCLUSION

Strong winds, observed in the east and south of the track of Typhoon-18 Songda were asymmetric and the wind stress vector turned clockwise through time. The maximum wind could induce net movement of surface water at about 90 degrees to the right of the surface wind direction in the Northern Hemisphere. Asymmetrical-cyclonic strong surface winds maximized surface divergence, which induced upwelling of deep colder sea water to the sea surface and its spreading outwards. Thus, asymmetrical SST responded to the tropical cyclonic wind forcing with the greatest cooling over the southeastern sea of Cheju Island along the typhoon track.

Simultaneously, a negative maximum geopotential tendency of 500 hPa for 24 hours was detected in the typhoon eye and its vicinity, while a positive maximum geopotential
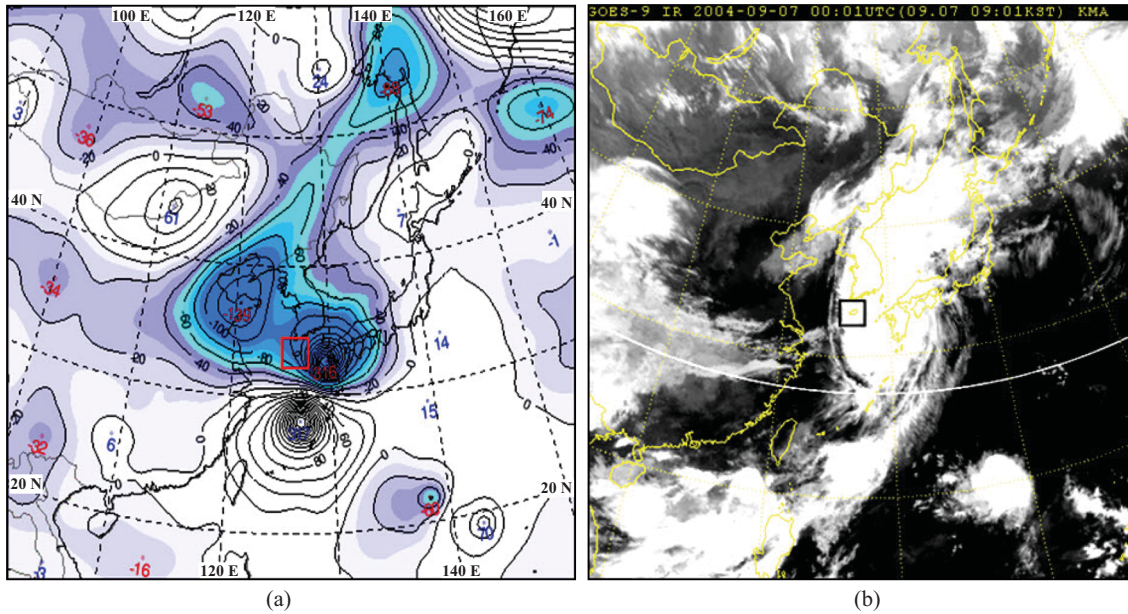
(a)   (b)

Fig. 10. As shown in Fig. 8, except for (a) 500 hPa height change for 24 hours at 0900 LST, September 7, 2004 and (b) GOES-9 satellite infrared cloud image. Typhoon Songda became Tropical Depression. White (blue) color area near Cheju Island denotes the increase (decrease) of geopotential tendency with a maximum of +317 m/day (-316 m/day) and a slope height of 633 m/day between two maxima. The typhoon turned toward northeast and passed by Korea Strait.
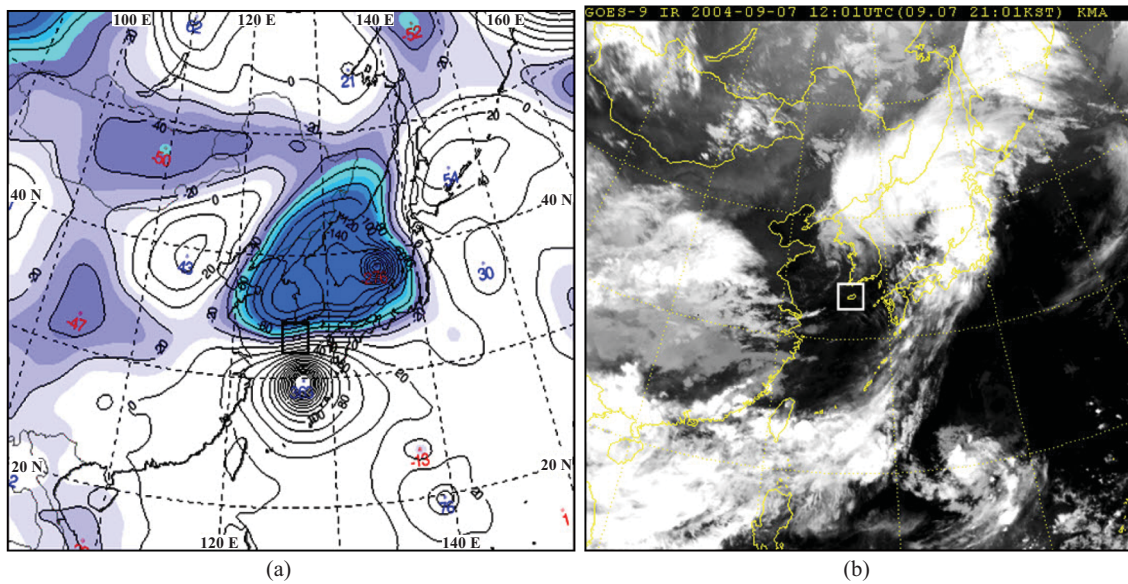

(a)   (b)

Fig. 11. As shown in Fig. 8, except for (a) 500 hPa height change for 24 at 2100 LST, September 7, 2004 and (b) GOES-9 satellite infrared cloud image. Typhoon Songda became an extra-tropical cyclone in the East Sea of Korea. White (blue) color area near Cheju Island denotes the increase (decrease) of geopotential tendency with a maximum of +363 m/day (-276 m/day) and a slope height of 639 m/day between two maxima. Positive geopotential tendency induces upwelling and outward spreading of deep sea colder waters along the inclined sea surface which cause cooling of surface waters in the south of Cheju Island along the typhoon track (Fig. 4(b)).

tendency was also detected behind the typhoon center along its track. The slope heights of 422 to 639 m/day between two maxima of negative and positive geopotential tendencies at 500hPa resulted in the elevation of the sea surface level and a large upwelling and outward spreading of deep cold sea waters along the inclined sea surface. As a result, the SST of 27°C reduced to 25°C over the sea southeast of Cheju Island along the typhoon track.

REFERENCES

1. Anthes, R. A. and Chang, S. W., "Response of the hurricane boundary layer to changes in sea surface temperature in a numerical model," *Journal of Atmospheric Sciences*, Vol. 35, pp. 1240-1255 (1978).

2. Babin, S. M., Carton, J. A., Dickey, T. D., and Wiggert, J. D., "Hurricane-induced phytoplankton blooms in the Sargasso Sea," *Proceeding of the 2002 AGU/ASLO Ocean Sciences Meeting*, American Geophysical Union, Honolulu, Hawaii (2002).

3. Cheung, T. C. and Chan, P. W., "Improving wind and rain simulations for tropical cyclones with the assimilation of Doppler radar data," *Proceeding of the 10th Annual WRF Users' Workshop*, Boulder, Colorado, pp. 1-835 (2009).

4. Choi, H., "Extreme cold sea outbreak near Cheju Island, Korea by strong wind and atmospheric pressure change under typhoon Rusa," *Disaster Advances*, Vol. 3, No. 1, pp. 32-41 (2010).

5. Choi, H., Choi, D. S., and Choi, M. S., "Heavy snowfall by orography and wind shift in cold front crossing Korean eastern coast," *Disaster Advances*, Vol. 2, No. 4, pp. 48-60 (2009).

6. Cione, J. J. and Uhlhorn, E. W., "Sea surface temperature variability in hurricanes: Implications with respect to intensity change," *Monthly Weather Review*, Vol. 131, pp. 1783-1796 (2003).

7. Elsner, J. B., "Tracking hurricanes," *Bulletin of American Meteorological Society*, Vol. 84, No. 3, pp. 353-356 (2003).

8. Gilbes, F., Armstrong, R. A., Webb, R. M. T., and Muller-Karger, F. E., "SeaWiFs helps asses hurricane impact on phytoplankton in Caribbean Sea, Eos, Transactions," *American Geophysical Union*, Vol. 82, pp. 529-533 (2001).

9. Gill, A. E., *Atmosphere-Ocean Dynamics*, Academic Press, New York (1982).

10. Holton, J. R., *An Introduction to Dynamic Meteorology, 4th Ed.*, Academic Press, New York (2004).

11. Hong, S. Y. and Lim, J. O., "The WRF single-moment 6-class microphysics scheme (WSM6)," *Journal of Korean Meteorological Society*, Vol. 42, pp. 129-131 (2006).

12. Kantha, L. H. and Clayson, C. A., *Small-Scale Processes in Geophysical Fluid Flows*, Academic Press, New York (2000).

13. Knauss, J. A., *Introduction to Physical Oceanography, 2nd Ed.*, Waveland Press, Illinois (2005).

14. Leipper, D. F., "Observed ocean conditions and Hurricane Hilda," *Journal of Atmospheric Sciences*, Vol. 24, pp. 182-196 (1967).

15. Monaldo, F. M., Sikora, T. D., Babin, S. M., and Sterner, R. E., "Satellite imagery of sea surface temperature cooling in the wake of Hurricane Eddouard," *Monthly Weather Review*, Vol. 125, pp. 2716-2721 (1997).

16. Price, J. F., "Upper ocean response to a Hurricane," *Journal of Physical Oceanography*, Vol. 11, No. 2, pp. 153-175 (1981).

17. Reed, R. J., "Cyclogensis in polar air stream," *Monthly Weather Review*, Vol. 107, pp. 38-52 (1979).

18. Reed, R. J. and Albright, M. D., "A case study of explosive cyclogenesis in the Eastern Pacific," *Monthly WeatherReview*, Vol. 114, pp. 2297-2319 (1986).

19. Reed, R. J. and Sanders, F., "An investigation of the development of a mid-tropospheric frontal zone and its associated vorticity field," *Journal of Meteorology*, Vol. 10, pp. 338-349 (1953).

20. Roberson, J. A. and Crowe, C. T., *Engineering Fluid Mechanics, 2nd Ed.*, Houghton Mifflin Company, Massachusetts (1976).

21. Sanders, F. and Gyakum, J. R., "Synoptic-dynamic climatology of the bomb," *Monthly Weather Review*, Vol. 108, pp. 1589-1606 (1980).

22. Sheng, J., Zhai, X., and Greatbatch, R. J., "Numerical study of the storm-induced circulation on the Scotian Shelf during Hurricane Juan using a nested-grid ocean model," *Progressive Oceanography*, Vol. 70, pp. 233-254 (2006).